Stability and Control for a Class of Dynamic Legged Climbers

Kevin Oishi

CMU-RI-TR-06-20

May 2006

Robotics Institute
Carnegie Mellon University
Pittsburgh, Pennsylvania 15213

Submitted in partial fulfillment of the
requirements for the degree of
Master of Science in Robotics

Abstract

We are interested in the stability and control of dynamic legged climbing. Motivated by the success of the lateral leg spring (LLS) and spring-loaded inverted pendulum (SLIP) templates for transverse and sagittal plane running on horizontal surfaces, our effort is to similarly approximate the analytically intractable dynamics of a full dimensional system through planar models, and develop simple control strategies based on analysis of these approximations. In this report we introduce low-dimensional generalizations of the LLS and SLIP templates capable of ascending and descending by considering configurations of the center of pressure outside of the set of asymptotically stable configurations in the horizontal plane, and allowing a thrust phase to add or remove energy from the hopper. We will provide mathematical analysis of these models where possible, and introduce approximate models and empirical data where analytical analysis is intractable. Stable control strategies developed from these low dimensional templates and approximations are demonstrated through simulation.

Contents

1   Introduction

Consider a scenario in which a person is jogging on an even, smooth sidewalk, which abruptly slopes or even becomes a rough gravel surface. The person's transition is typically smooth and arguably involves very little active control–the act of walking remains a largely repetitive task that requires relatively little thinking. However, such transitions in robotic systems remain difficult. Successful implementations of legged mobile robots are often sensitive to terrain, and must be finely tuned or equipped with extensive sensing and control capabilities. Both of these limitations must be overcome for the next generation of dynamic legged robots to be both robust to terrain and simple to control.

Appropriate level of model fidelity, as well as simple control mechanism, are inherent to the robustness and success of any given dynamic legged robot. Initial approaches by control theorists and biologists have involved complex, nonlinear behaviors which can arise from simple, mechanistic models. The main challenge in this arena has been to create models which are both physically accurate and analytically tractable.

Despite extensive work in modeling, analysis, and control of legged robots on flat ground, little work has been done to achieve this same success on sloped terrain. Although we now have basic design strategies for dynamic legged systems on flat ground, methods for dealing with slopes and climbing are limited to treating the effects of a slope as isolated perturbations. The fact that we are interested in dynamic legged locomotion exclusively on a slope breaks the assumptions that lead to asymptotically stable running on level ground. Still, we hypothesize that simple and even open-loop control can be a viable strategy for dynamic legged systems on a slope. In this report we seek to resolve this gap by presenting the first analytic work suggesting a design strategy for stable and robust dynamic legged climbers requiring little or no sensing.

1.1   Previous Work

Raibert's seminal work in hopping robots [1] is considered the first example of robotic dynamic legged locomotion. Essentially an actuated pogo sticks, Raibert's hoppers modeled only one leg, but provided immense utility for control theorists and biologists interested in the stability and control of legged locomotion. Although limited in its scope, the hoppers emulated a variety of behaviors observed in actual biological systems. By modulating leg touch-down angle and thrust duration, Raibert showed empirically stable hopping utilizing simple controllers built around the approximation of decoupled forward velocity and hopping height. Researchers building upon his benchmark model further explored the stability of legged running and the coupling between forward velocity and hopping height for a class of simplified models of Raibert's hoppers termed the spring-loaded inverted pendulum (SLIP).

Control theorists approximated the SLIP return map, the function mapping hopper height and forward velocity of at the apex of one hop to the apex of the following hop. For certain nonlinear springs, this map was shown to fall into the class of S-Unimodal functions, guaranteeing asymptotic stability for certain period-1 gaits where the hopper returned to the same height and forward velocity at each apex [2]. Chaotic attractors were found [3], and bifurcation diagrams supported the stable period-2 "limping" gaits

observed in Raibert's hoppers [4] where a small hop was succeeded by a large hop, or vice versa. Simultaneously, biomechanics researchers have explored the SLIP model in biological systems [5]. Blickhan and Full surveyed a variety of legged animals, finding the SLIP model to be an accurate representation of the center of mass dynamics in the sagittal plane [6]. In more explicit collaboration, biologists and control theorists studied the neurological control of certain legged animals [7] and illustrated methods for quantifying stability and maneuverability for legged animals [8]. These studies led to an investigation of transverse plane dynamics in multi-legged biological systems. Control theorists dubbed this new model, based on the SLIP, the lateral leg spring (LLS).

The lateral leg spring is essentially SLIP turned on its side. Rather than a pogo stick bouncing up and down, LLS is a pogo stick bouncing between the walls of an imaginary corridor. While SLIP models the up-and-down motions of a legged runner, LLS is an attempt at distilling the important components of side-to-side running dynamics in multi-legged animals. If LLS is a pogo stick bouncing between the walls of a corridor, then the wall positions and curvature of this corridor are determined by the location and orientation of the sideways pogo stick at the arbitrary moment the "foot" is attached to the ground. Control theorists and biologists building on this model have determined the relationship between body geometry and stable locomotion in terms of heading (the straightness of the imaginary corridor) as well as overall forward velocity in terms of body geometry for open-loop gaits [9, 10].

One might wonder about the effectiveness or purpose of developing control strategies for idealized systems. In fact, control strategies developed for the idealized SLIP and LLS models have translated well into real systems. Robotic platforms, such as RHex the robotic hexapod have been shown to exhibit SLIP and LLS stability [11], and benefit from control strategies developed for parameter-matched models [12, 13, 14, 15, 16]. It is important to stress that the goals of control theorists and biologists are not always the same. Historically control theorists studying legged locomotion have the design of an engineered system in mind, while biologists have typically been primarily interested in learning how animals locomote. However, it is interesting to note that in many cases biologists have gone back and validated mathematical results of the lateral leg spring stability through experiments on legged animals [17, 10, 8].

1.2   Method and Contributions

Models of dynamic running are mechanically elegant, but mathematically complex and difficult to treat analytically. Our work focuses on stability and control for dynamic legged locomotion along sloped and vertical surfaces by decomposing the full dimensional climber into planar models, and studying the dynamics of these planar models. It has been shown analytically, and verified experimentally, that under certain control laws and body configurations, dynamic legged runners based on the planar hybrid SLIP and LLS models are guaranteed to converge on certain periodic trajectories when perturbed, even with little or no sensing. Unfortunately, the pervading simplifying assumptions leading to these results preclude progress into a gravity field, and dynamic legged climbing remains a largely unexplored problem. This report seeks to address this problem by generalizing LLS and SLIP models to add and remove en-

ergy to enable ascending and descending, while keeping these models simple enough to allow analytic analysis where possible.

The main contribution of this thesis involves the modeling, analysis, and simulation of four models of dynamic legged locomotion:

1. LLS Peg-Leg Climber

    (a) New model of transverse plane dynamics of a climber on a slope.

    (b) Analytic conditions for heading stability for open-loop climbers based on this model.

2. LLS Simplified Hexapod Climber

    (a) New model of transverse plane dynamics of a climber on a slope, capable of more complicated behaviors than the LLS peg-leg climber, though analytically difficult.

    (b) Empirical evidence of the limits of heading stability on sloped surfaces through simulation.

3. SLIP 2-DOF Hopping Climber

    (a) New model of sagittal plane dynamics of a climber on a slope.

    (b) Numerical study of the stability of this climber through simulation.

4. SLIP 1-DOF Model and Approximation to the 2-DOF Hopping Climber

    (a) New model of sagittal plane dynamics of a climber on a slope representing the singular, vertical, climbing mode in the 2-DOF hopping climber.

    (b) Closed-form return map for a class of 1-DOF vertical climbers.

    (c) Identification and classification of the fixed points of the general 1-DOF climber.

    (d) Empirical evidence suggesting the robust asymptotic stability of the 1-DOF climber.

    (e) Empirical evidence suggesting the viability of the 1-DOF climber as an approximation to the intractable 2-DOF hopping climber and, by proxy, a simple control law for stable climbing.

1.3   Organization

Section 2 provides the reader with a brief tutorial in hybrid dynamic systems. This section provides the mathematical framework for the analysis of hybrid dynamic legged climbers. We then decompose the full-dimensional climber into planar approximations, in order to discern properties of stability and control. In Section 3 we present transverse planar dynamics through an extended LLS model. In Sections 4 and 5 we approximate sagittal planar dynamics through an extended SLIP model. In each section, we describe a particular planar approximation, discuss its dynamics, and then analyze the model for

its stability, despite minimal sensing and control. In the case that analytic results are not possible, we alternatively provide empirical studies through simulation.

The discussion of transverse plane dynamics begins in Section 3 with the standard, flat-ground LLS model. We extend this model to capture heading dynamics and progress against a slope. Building upon a stability argument for the original level ground LLS model, the body-geometry conditions for stability in a gravity field under an open-loop controller are derived. Resulting stable trajectories are classified, and limitations of climbers based on this model are discussed. Section 4 continues the exploration of LLS models, introducing a more complicated, and analytically difficult hexapod model. Empirical study of this model hints at limitations and illustrates significant advantages in stability as compared to the peg-leg LLS climber.

The discussion of sagittal plane dynamics begins in Section 4 with the standard, level-ground SLIP model. We extend this model initially to a 2-DOF hopping climber. Unfortunately, as is typical of SLIP-based models, the explicit analytic integration of stance dynamics in order to compute return maps requires computation of elliptical integrals, making it analytically intractable. Methods for solving this problem in level ground rely on approximations which ignore gravity during stance or require symmetry in stable trajectories, making these techniques inappropriate in a sloped or vertical domain. To solve this problem we suggest using the singular vertical mode of the 2-DOF hopping climber as an easily integrated 1-DOF approximation. A Poincaré section for hopping climbers is introduced, and fixed points for a representative climber are found and classified. Stability properties of the 1-DOF hopping climber are discussed, and empirical evidence suggesting the strength of the approximation to the intractable 2-DOF model is presented. Section 6 concludes the report with a discussion of possible applications of this research and directions for future work.

2 Legged Climbing as a Hybrid Dynamical System

We begin by describing a general model of legged climbing and present this model in the framework of hybrid systems. Later, specific models of legged climbing will be introduced and analyzed in this setting.

Models for the peg-leg runner in a gravity field and 2-DOF hopping climber are illustrated in Fig. 2 and Fig. 13, respectively. For a general climber, a single stride is comprised of several discrete transitions between different sets of constraints, making the model of a legged climber a hybrid system. This means that the dynamics of a legged climber cannot be represented by a single flow. Instead, the trajectory of a climber is computed from piecewise integration over a collection of vector fields, with discrete transformations guiding transitions between vector fields.

Similar to many horizontal legged running models, the dynamics of the legged climber segments into two major phases, flight and stance [15, 8]. In a sagittal plane model, energy can be added or removed during stance by further decomposing stance into three sub-phases, compression, thrust, and decompression [4]. In the framework of hybrid systems, significant points in the trajectory of the climber, for example phase transitions, can be represented as zero-crossings in functions of state and time. These functions are referred to as threshold functions, and the zero-crossings are called

events.

Borrowing notation from Altendorfer [12], we can more precisely describe the mathematical framework of the model. Let I be a finite index set and X_α, $\alpha \in I$ with $\dim(X_\alpha) = 2N$, $N \in \mathbb{N}$ be a collection of charts, Euclidian spaces describing the phase space of a constrained system. Suppose we have some system with $\mathbf{q}$ a variable in configuration space and $\mathbf{x} = \begin{bmatrix} \mathbf{q} & \dot{\mathbf{q}} \end{bmatrix}^T$ a variable in phase space. The vector field $f_\alpha : \mathbf{x} \mapsto \dot{\mathbf{x}}$ can be integrated to obtain the flow $f_\alpha^{(\cdot)} : X_\alpha \to X_\alpha$. Given the initial condition $\mathbf{x}_0 \in X_\alpha$ and integration time $t \in \mathbb{R}$, $\mathbf{x}(t) = f_\alpha^t(\mathbf{x}_0)$. Suppose $\beta \in I$ with $\beta \neq \alpha$. Each phase corresponds to the equations associated with an element of the index set I. The transition from f_α to f_β corresponds to the threshold function $h_\alpha^\beta : (X_\alpha, \mathbb{R}) \to \mathbb{R}$. Given initial conditions $\mathbf{x}_0$, the next transition event occurs at the time $t_\alpha(\mathbf{x}_0) = \min_{t>0} \left\{ t : h_\alpha^{(\cdot)}(\mathbf{x}_0, t) = 0 \right\}$. Put together, this yields the flow map $F_\alpha : \mathbf{x}_0 \mapsto f_\alpha^{t_\alpha(\mathbf{x}_0)}(\mathbf{x}_0)$. Finally, the discrete transformations between charts are denoted $T_\alpha^\beta : X_\alpha \to X_\beta$. In this paper, unless otherwise noted, this transformation is simply the identity. We will use the index set $\{\mathbf{f}, \mathbf{s}, \mathbf{c}, \mathbf{t}, \mathbf{d}\}$ to refer to flight, stance, compression, thrust, and decompression, respectively.

As suggested by the notation in Fig. 2 and Fig. 13, the trajectory of a legged climber can be considered periodic. Within certain bounds, trajectories are defined on a recurring series of charts. A single stride is described by the composition of flow maps and discrete transformations associated with a single cycle through these charts. It should be noted that unlike level ground running, not all of the dimensions of phase space are essential in describing the dynamics of locomotion; for example, in models described in this paper, total system energy and distance along the slope traveled are extraneous to describing the dynamics of climbing. By projecting down to capture only essential dimensions, certain trajectories of legged climbers become periodic orbits. We are interested in the stability or attractiveness of these orbits, and will explore these properties empirically and analytically through numerical integration and studying the differential behavior of the orbit.

3 Inclined-LLS: Peg-Leg Runner in a Gravity Field

Schmitt and Holmes [9, 14] first presented the lateral leg spring (LLS) model, which has been used to characterize the transverse plane dynamics of cockroaches [8] as well as multi-legged robots like RHex [11] over level ground. The basic idea is that for a given gait with a well defined "left side" and "right side," the legs in contact with the ground during stance can be modeled as a single effective spring-leg. The effective spring-leg is attached to the ground during stance via a frictionless pin joint at the foot. In this way a two-sided gait could be likened to bouncing between effective left and right spring-legs.

Schmitt and Holmes also showed that under certain conditions, the dynamics of the LLS model are reflected in a simpler "peg-leg" model [9]. In the peg-leg model, the spring-leg is replaced with a rigid foot constrained to move along the lateral axis of symmetry, attached to the body by a prismatic joint. A single stride consists of a stance phase and zero-duration flight phase. During stance the foot is attached to the ground
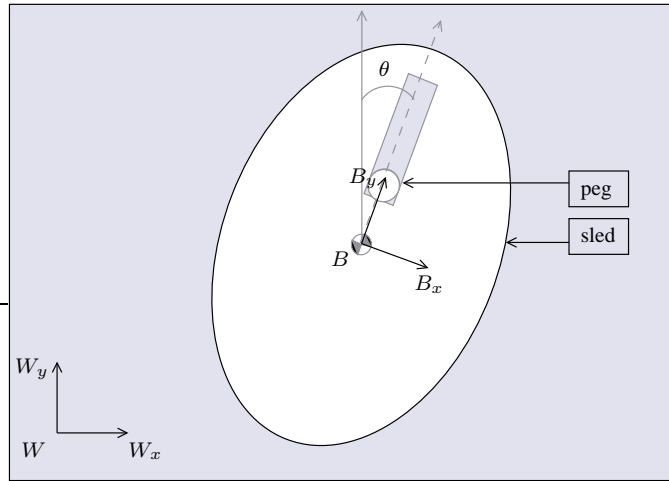
Figure 1: Peg-leg body geometry. Position in the world frame and body frame are given in Cartesian coordinates (W_x, W_y) and (B_x, B_y) respectively. The origin of the body frame is at the center of mass. Position of the peg is measured as the distance along B_y from the center of mass to the peg. Note the isometry between positive and negative peg positions. The angle between B_y and W_y is measured by θ. In the climbing peg-leg model it is assumed that the gravity vector points in the $-W_y$ direction.

by a frictionless pin joint moving from some starting position to some ending position relative to the body center of mass and orientation. At flight the foot is instantaneously repositioned at the new starting position. One way to visualize this stride is to imagine a sled without runners on a frozen lake, with a slot cut out along the lateral axis of symmetry. An illustration of this sled is shown in Fig. 1. A person riding on the sled (at the center of mass) is given an ice pick, and allowed to move by repeating three simple movements:

1. Stab the ice pick into the ice at one end of the slot.

2. Push or pull the ice pick until it is at the opposite end of the slot.

3. Remove the pick from the ice and reposition it at the beginning of the slot.

In the horizontal case, the peg-foot can be thought of as the center of pressure of the spring-leg LLS model. A key result of this model is that under reasonable body-geometry assumptions and certain open-loop gaits, the angular momentum of the body will asymptotically approach zero, meaning the runner will converge on a particular heading. This global stability result is reflected in empirical studies of running cockroaches and the robot hexapod RHex [8, 11].

Inspired by the simplicity and success of this peg-leg model, the natural starting place in our study of climbing dynamics is to pitch the peg-leg runner into a gravity field, as illustrated in Fig. 2.

6
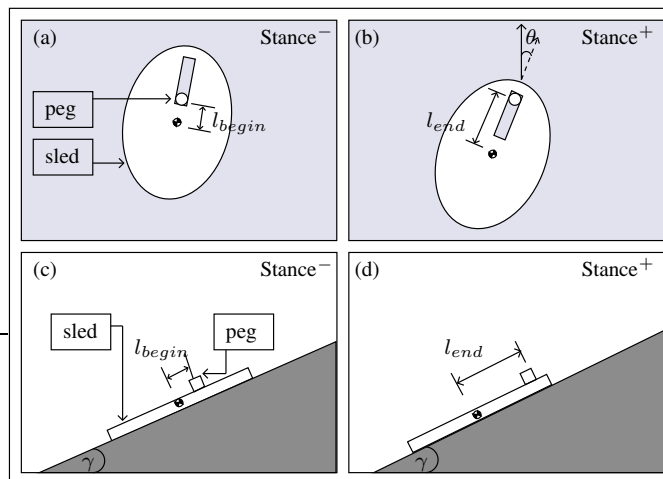
Figure 2: Peg-leg climber during stance. (a)-(b) Top view. (a) Beginning of stance. θ is measured with respect to the climbing surface gradient. In this figure the gradient of the climbing surface points along the length of the page. (b) End of stance. The sled has translated and rotated about the fixed peg position. (c)-(d) Side view. (c) Beginning of stance. The angle of the planar climbing surface relative to gravity is γ. (d) End of stance.

3.1 Dynamics

To simplify dynamics, the climber is assumed to have a planar rigid body, symmetric about the sagittal axis with mass m and moment of inertia I. The climber operates in a gravity field of magnitude g, along a planar climbing surface γ-degrees from horizontal. Body angle θ is measured relative to the climbing surface gradient. The coordinate systems and frames of reference used describing this model is illustrated in Fig. 1. The origin in body coordinates is located at the center of mass. As in the horizontal peg-leg model, the body is equipped with a slot running along the sagittal axis of symmetry. In Cartesian body coordinates (B_x, B_y), this slot begins at $(0, l_{begin})$, and ends at $(0, l_{end})$. As in the horizontal peg-leg model, movement is effected through a massless peg-leg that can be fixed to the running surface and moved relative to the body along the slot. We assume the sled is frictionless with respect to the ground and peg, and the point of contact between the peg and ground acts as a frictionless pin joint. Control is exerted only during stance through the position of the peg, l, relative to the center of mass along the B_y body frame axis.

3.1.1 Flight

During flight the climber slides without friction along the climbing surface subject only to gravity. Although in our analysis we consider the duration of the flight phase to be zero, we include the equations of motion here for completeness. The peg is instantaneously repositioned at $(0, l_{begin})$ in body coordinates when the climber transitions

from flight to stance. This change in configuration results in a discrete jump in angular velocity due to the conservation of angular momentum.

$$\ddot{\theta} = 0 \tag{1}$$

$$h_{\mathbf{f}}^{\mathbf{s}}\left(\mathbf{x}, t\right) = 0 \tag{2}$$

$$T_{\mathbf{f}}^{\mathbf{s}} = diag(1, \frac{ml_{begin}l_{end} + I}{ml_{begin}^2 + I}) \tag{3}$$

3.1.2 Stance

During stance the climber slides without friction along the climbing surface, subject to gravity and the prescribed position of the peg. In our model we assume the peg position as a function of time $l(t)$ to be periodic and strictly monotonic during stance. Stance ends when the peg reaches the opposite end of the slot.

$$\ddot{\theta} = ml \left(\frac{g \sin \gamma \sin \theta - 2\dot{l}\dot{\theta}}{I + ml^2} \right) \tag{4}$$

$$h_{\mathbf{s}}^{\mathbf{f}}\left(\mathbf{x}, t\right) = l_{end} - l \tag{5}$$

3.2 Stability in the Peg-Leg Climber

As with the horizontal peg-leg runner, an easy way to visualize the climbing stride is to imagine an ice-pick driven sled without runners on a frozen slope. Schmitt and Holmes showed that on level ground for certain body geometries an open-loop controller can force the sled to converge on some heading θ [9, 14]. We would like to determine if there is a similar stability property for the peg-leg climber.

In the horizontal running case, angular momentum about the peg is conserved during stride. At the beginning of each new stride the instantaneous change in peg position causes an angular impulse and a discrete jump in angular velocity, which can be modeled as a linear transformation. In Schmitt and Holmes' argument [9], this transformation is expressed in terms of angular momentum. The integrated stance dynamics also reduces to a linear function of angular momentum, meaning the stability of a particular runner is determined simply from the eigenvalues of the linear return map.

In the vertical running case the discrete jump in angular velocity between strides (3) is the same as in the horizontal case. Introducing a gravity field explicitly breaks the assumption that angular momentum is constant about the peg during stance, and leads to a nonlinear stride map. Taking a closer look at stride dynamics, we see the effect of stride on angular momentum.

$$\frac{\partial \ddot{\theta}}{\partial l} = \frac{m \left(I - ml^2\right) \left(g \sin \gamma \sin \theta - 2\dot{l}\dot{\theta}\right)}{\left(I + ml^2\right)^2} \tag{6}$$

$$\frac{\partial \ddot{\theta}}{\partial \dot{l}} = \frac{-2ml\dot{\theta}}{I + ml^2} \tag{7}$$

Without loss of generalization, let $l > 0$. Combining (4) and (6) we see that

$$\text{sign}\left(\Delta\ddot{\theta}\right) = \text{sign}\left(\ddot{\theta}\left(I - ml^2\right)\Delta l\right) \tag{8}$$

There are three cases to consider:

1. If $I = ml^2$, then change in l has no effect on angular acceleration.

2. If $I < ml^2$, then the magnitude of $\ddot{\theta}$ increases when $\dot{l} > 0$ and decreases when $\dot{l} < 0$.

3. If $I > ml^2$, then the magnitude of $\ddot{\theta}$ decreases when $\dot{l} > 0$ and increases when $\dot{l} > 0$.

From (7) we see that

$$\text{sign}\left(\Delta\ddot{\theta}\right) = \text{sign}\left(-\dot{\theta}\Delta\dot{l}\right) \tag{9}$$

Again there are three cases to consider:

1. If $\ddot{l} = 0$, there is no effect on angular acceleration.

2. If $\ddot{l} < 0$, then the leg is accelerating toward the center of mass, and there is a change in angular acceleration in the direction of rotation.

3. If $\ddot{l} > 0$, then the leg is decelerating in the direction of the center of mass, and there is a change in angular acceleration against the direction of rotation.

Essentially we have just shown the "figure skater" result in a gravity field. Like a horizontally rotating object with adjustable mass positions, pulling mass toward the pivot point increases angular acceleration, while pushing mass away from the pivot point decreases angular acceleration. Since we are on a slope, the direction of angular acceleration depends on gravity.

For a large class of foot trajectories, such as constant velocity during stride, as illustrated in Fig. 3, we can construct a bound on angular acceleration for a stride as a function of angular momentum at the beginning of the stride. This bound leads to a familiar bound on angular momentum, subject to the same stability properties seen in the horizontal runner.

Unlike the horizontal runner, the stance dynamics leads to only four fixed points unique up to isomorphism. Three of these points are marginally stable and one is asymptotically stable. When pulling the sled there are two marginally stable fixed points:

1. Pulling with $\dot{\theta} = 0$ and a heading which climbs the surface gradient is marginally stable.

2. Pulling with $\dot{\theta} = 0$ and a heading which descends the surface gradient is marginally stable.

When pushing the sled there is one marginally stable fixed point and one asymptotically stable fixed point:

9
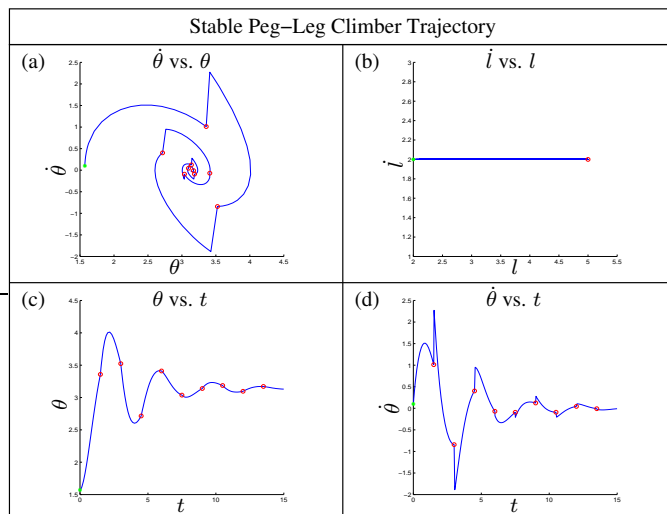
Figure 3: Trajectory of a stable peg-leg climber. System parameters are defined as $l_{begin} = 3, l_{end} = 5, \dot{l} = 2, \theta_0 = \frac{pi}{2}, \dot{\theta}_0 = 0.1$. Note there is an isometry between this climber and one where $l_{begin} = -3, l_{end} = -5$, and $\dot{l} = -2$. Points on the trajectory denote the beginning of the run and the end of stance phases. Note the discrete jumps in angular velocity following the end of each stance. (a) Phase plane plot of the stable climber. (b) Leg trajectory for this climber. (c) The angle θ as a function of time. (d) $\dot{\theta}$ as a function of time.

1. Pushing with $\dot{\theta} = 0$ and a heading which climbs the surface gradient is marginally stable.

2. Pushing with $\dot{\theta} = 0$ and a heading which descends the surface gradient is asymptotically stable.

Regardless of the gravity field, we see that heading is asymptotically stable only when the slot is entirely behind the center of mass and the peg "pushes" away from the center of mass during stance. However, because our model explicitly accounts for the effect of gravity, we see that only descending is asymptotically stable–ascending is only marginally stable. This result shows the importance of including gravity in models of legged locomotion. The simple peg-leg model which adequately models transverse plane dynamics over flat-ground is missing important complexities necessary for climbing. In fact, a brief exploration of a more complex open-loop leg-spring model confirms that it is possible to ascend a slope or vertical surface with asymptotic stability on heading.

3.3 Initial Experimental Results

In our experiments we focus on two distinct methods of legged locomotion derived from experimentally designed robots RHex and RiSE, and test the effectiveness of

these climbing methods through simulation in the context of the peg-leg climber. Both RHex and RiSE are symmetric hexapods with compliant legs, and are capable of locomotion through alternating tripod gaits, meaning that left and right legs work in conjunction to form alternating and symmetric tripods. Though RHex and RiSE share some similarities, their motivated design goals are very different.

RHex was designed for flat-ground running. RHex bounces from tripod to tripod with heading stability of a LLS model. Abstracting away details like duty cycle and precise model parameters, we view this style of bouncing legged locomotion of as a possible method for climbing inclined planes. Alternatively, RiSE was designed to climb extreme slopes, and remaining firmly attached to the wall is important for this method of legged locomotion. In an alternating tripod gait, RiSE firmly attaches itself to the substrate with each tripod, releasing only once the opposite tripod has attached.

Using a relatively high-fidelity dynamic hexapod model developed by Seipel, Full, and Holmes [10] which has been shown to exhibit LLS stability for certain open-loop controllers on flat ground, we will make sleight modifications, introducing a gravity field and changing the stride switching function, in order to implement and test the effectiveness of both RHex and RiSE climbing methods in terms of heading stability as a function of model parameterization and climbing slope.

3.3.1 Dynamics

The level-ground hexapod body geometry and coordinate systems are illustrated in Fig. 4 [10]. The basic idea is that tripods formed by hip-leg-foot sets 1,2,3 and 4,5,6 alternate and symmetrically drive the body through effective spring-resting length and hip position during stance with a nominal frequency of f. Though the model shares some simplifying assumptions with the peg-leg runner, it remains extremely complex and difficult to treat analytically. The body is assumed to be rigid with mass m and moment of inertia I. In the Fig. 4, θ measures the orientation of the body (heading) relative to the y inertial axis, while δ measures the direction of the velocity of the center of mass relative to the y inertial axis. The body consists of 6 slots which constrain the movements of six hips. Drawn individually for clarity in the figure, the hips and slots are actually collinear, located along the longitudinal axis of symmetry, passing through the center of mass. Hip, leg, and foot configurations are indexed according to the figure. The location of each hip along the $e2$ body axis relative to the center of mass is denoted d_i. Each hip is attached to a linear spring-leg with spring constant k_i and resting length l_i. The vector from the foot to the hip is denoted $\mathbf{q}_i$. The position of each foot relative to the center of mass in body coordinates $(e1, e2)$ at the beginning of stance is given by $\mathbf{b}_i$. The position of the center of mass in the inertial frame is denoted $\mathbf{r}$.

Control is open-loop, and exerted during stance through the spring-leg resting length l_i and position of the hip d_i, which are computed ahead of time to match an idealized sinusoidal foot force profile and desired fore-aft velocity V_d. In their paper, Seipel, Full, and Holmes parameterized their model to match idealized sinusoidal foot forces measured from running cockroaches, and we follow their parameterization, illustrated in Fig. 5 [10].

In our model, we explicitly account for the force of gravity g, which acts along the $-y$ inertial axis, and a climbing surface with slope σ. We denote the force on the

11
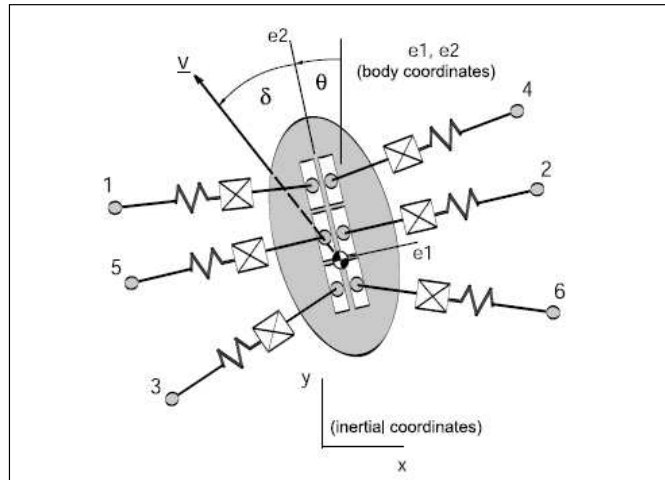
Figure 4: Seipel, Full, and Holmes' hexapod body geometry [10]. Position in the inertial (world) frame and body frame are given in Cartesian coordinates (x, y) and $(e1, e2)$ respectively. In this figure $\bar{v}$ denotes the velocity of the center of mass. The angle between $\bar{v}$ and the y-axis of the world frame is expressed as δ. Similarly, the angle between the y-axis of the world frame and the $e2$-axis of the body frame is measured by θ. Hip, spring-leg, and foot configurations are indexed as illustrated in the figure. In this way 1,2,3 and 4,5,6 denote alternating tripod stances. For clarity, all 6 slots constraining hip movement are illustrated separately in this figure; however, in actuality the constraining slots are all collinear.
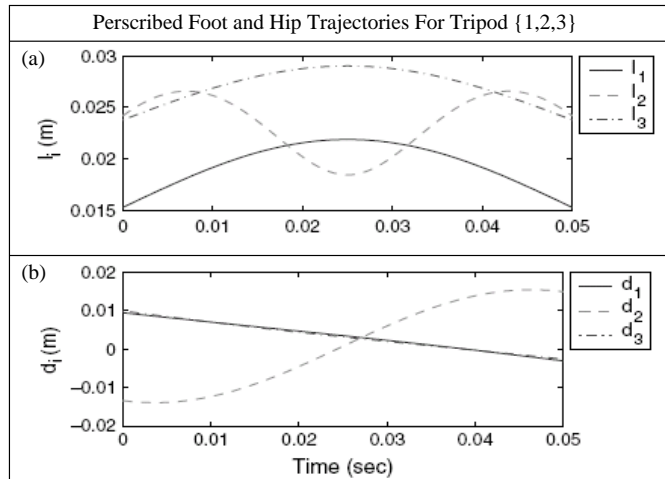
Figure 5: Prescribed foot and hip trajectories as presented by Seipel, Full, and Holmes, computed for the 1,2,3 tripod [10]. Note that the trajectories for the 4,5,6 tripod are identical except for the stride-frequency phase shift.

12

center of mass $\mathbf{F}$, the total moment about the center of mass $\mathbf{M}$, and the inertial frame x or y component of any vector value with a subscript x or y. With this notation, the equations of motion become:

$$m\ddot{\mathbf{r}} = \mathbf{F} \tag{10}$$

$$\mathbf{F}_x = \sum_i k_i \left(l_i - |\mathbf{q}_i| \right) \frac{\mathbf{q}_{ix}}{|\mathbf{q}_i|} \tag{11}$$

$$\mathbf{F}_y = \sum_i k_i \left(l_i - |\mathbf{q}_i| \right) \frac{\mathbf{q}_{iy}}{|\mathbf{q}_i|} g \sin \sigma \tag{12}$$

$$I\ddot{\theta} = \sum_i -\frac{d_i F_i}{|\mathbf{q}_i|} \left(q_{ix} \cos \theta + q_{iy} \sin \theta \right) \tag{13}$$

The stance threshold function has two forms, one for each climbing method. For the RHex climbing method switching is dependent on foot force minus the effect of gravity:

$$h_{\mathbf{s}}^{\mathbf{s}} \left(\mathbf{x}, t \right) = \min \left\{ k_i \left(|\mathbf{q}_i| - l_i \right) \right\} \tag{14}$$

For the RiSE climbing method, switching is dependent on stance time only.

$$h_{\mathbf{s}}^{\mathbf{s}} \left(\mathbf{x}, t \right) = \quad \mathrm{mod} \left(t, \frac{1}{f} \right) \tag{15}$$

3.3.2 RHex Configuration

This model is robust to perturbations to heading and velocity on flat ground, and shown by SFH to have a large basin of attraction for parameterizations in the neighborhood of measured values. On level ground, the model converges on a heading rapidly, as illustrated in Fig. 6 and Fig. 10.

In our experiments we run simulations of a particular hexapod with some initial conditions in the neighborhood of a stable flat-ground running parameterization over a range of slopes. Simulations are run in Matlab using default settings for the ode45 solver. Each run consists of 400 left-right strides to ensure stability. We compute the mean and variance of the heading for stabilized climbers, using only the last half of the time-ordered data set.

Data presented here is from a series of runs, each with the same initial conditions. Effectively plots conveying asymptotic heading are only showing half of the picture. In most cases, a small change, for example reversing the initial tripod stance (starting on the right side instead of the left), would result in a heading sign change.

We found that for a particular model parameterization, the limit heading is not arbitrary, and depends on the climbing slope. Data from a representative trial are illustrated in Fig. 8, which shows the mean and variance of the heading for a stabilized gait as a function of climbing slope. For the smallest slopes, heading converges on the climibng surface gradient–directly ascending the fall-line. This is followed by a range in σ where
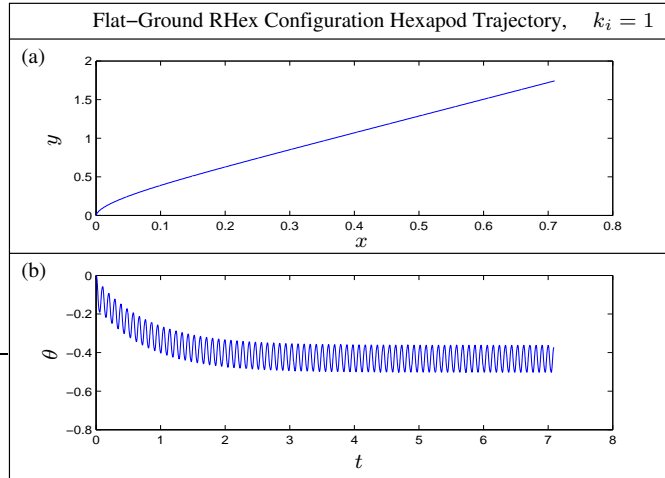
Figure 6: Trajectory of the flat-ground ($g = 0$) RHex Configuration hexapod, $k_i = 1$ for $i \in 1, 2, 3, 4, 5, 6$. (a) Trajectory of the center of mass in the (x, y) inertial frame. (b) Oscillatory trajectory of heading θ as a function of time. Note the rapid convergence about $\theta = -0.4$.
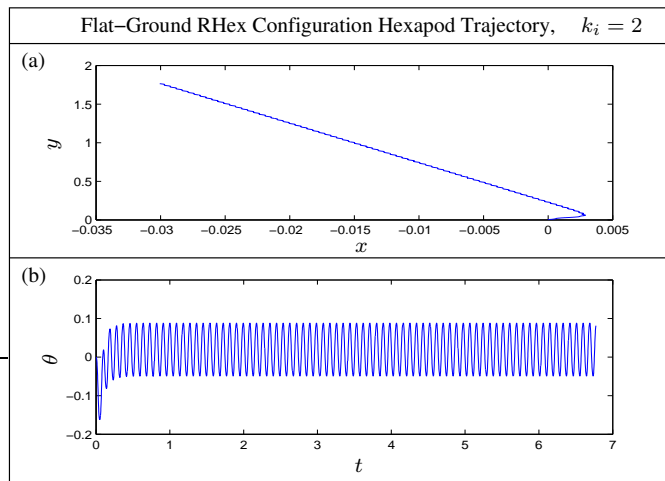
Figure 7: Trajectory of the flat-ground ($g = 0$) RHex Configuration hexapod, $k_i = 2$ for $i \in 1, 2, 3, 4, 5, 6$. (a) Trajectory of the center of mass in the (x, y) inertial frame. (b) Oscillatory trajectory of heading θ as a function of time. Note the extremely rapid convergence about $\theta = 0$.

14
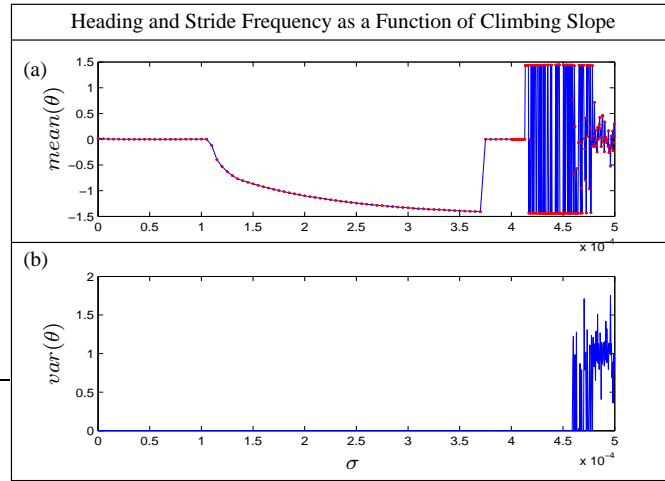
Figure 8: Heading beyond the range of stable climbing slopes for a RHex Configuration climber, $k = 2$, $g = 9.8$. (a) Heading is computed as the average θ over a series of strides for a stabilized climber. Note that this map represents a bifurcation diagram symmetric about $\theta = 0$. (b) The variance of θ correlates with stable bifurcations through $\sigma = 4.5 \cdot 10^{-4}$.

as slope increases the asymptotic heading skews from vertical, but never reaches an angle perpendicular to the climbing gradient. After this the heading abruptly returns to vertical before falling into a stable bifurcation at the limits of its skew climbing. Finally the climber reaches its maximum climbable slope, beyond which the trajectory falls into chaos, as shown by the heading variance.

3.3.3 RiSE Configuration

We reproduce similar experiments now with the RiSE Configuration. We use the same initial conditions as we did for the RHex Configuration in Section 3.3.2. In the analysis that follows, note that plots depicting heading or heading rate of change should be seen as half of a bifurcation which is symmetric about $\theta = 0$ or $\dot{\theta} = 0$.

For the RiSE configuration we experimented both on flat ground as well as an inclined slope. In our flat ground experiments RiSE Configuration climbers were allowed to run for 200 left-right strides each over a range of V_d values. Initial conditions we chosen in the neighborhood of stable flat-ground RHex Configuration parameterizations. This time, the mean angular velocity was computed from the last half of the time-ordered data set to ensure the data represented a stabilized runner.

We did not find a stable heading; however, despite being driven by a symmetric alternating tripod gait, we did find stable rates of heading change. In other words, although the climber did not run in a straight line, it did converge to stable circular paths, as illustrated in Fig. 9. Although this is not the same as heading stability as observed in LLS runners, we consider the similarity stability in angular velocity warrants further
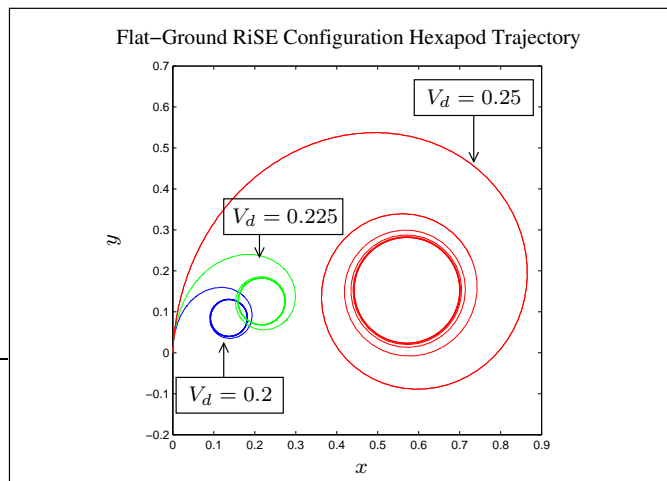
Figure 9: Trajectories of the center of mass of RiSE Configuration dynamic runners in Cartesian (x, y) world coordinates. The climber is parameterized with $k_i = 1$, $V_d = 0.25, 0.225, 0.2$. Note the stable circular trajectories of different curvatures. Initial conditions were a heading and forward velocity along the y-axis with no angular velocity component. In this case, starting with the "opposite foot" would lead to trajectories symmetric about the y-axis.

study. The curvature of these paths could be controlled by changing the parameter for desired velocity, V_d, in the open-loop controller. Plotting the mean angular velocity of stabilized gaits against V_d we found a characteristic unimodal function with clear minimum and maximum curvatures as shown in Fig. 10.

In our climbing experiments, we again ran the hexapod simulation for 500 left-right strides over a range of slopes using parameterizations in the neighborhood of those which produced stable gaits on level ground. Again, the mean and variance of heading are computed from only the last half of the time-ordered data for each run.

Curiously, we found that despite our flat-ground results the climber tended to directly ascend the slope gradient, except for a relatively small range of slopes near the edge of its stable region where the climber stabilized on minutely skew headings, as shown in Fig. 11. As with the RHex configuration, there is a limit to the range of climbable slopes for any particular model parameterization; however it is interesting to note that for identical parameterizations, the RiSE model appears to cover a greater range of slopes than the RHex Configuration.

4   Inclined-SLIP: 2-DOF Hopping Climber

While Section 3 focused on lateral dynamics, we now focus in Section 4 on the longitudinal. The extended SLIP model presented in this section builds upon previous flat-ground models of sagittal-plane dynamics, but directly incorporates the effects of

16
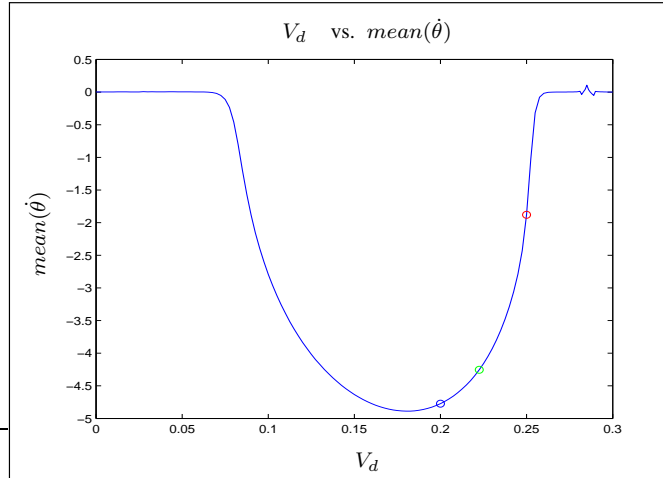
Figure 10: Mean heading as a function of V_d over level-ground, $k = 1$. Note the nearly unimodal behavior of this mapping with limits at $mean(\dot{\theta}) = 0$ for large and small values of V_d.
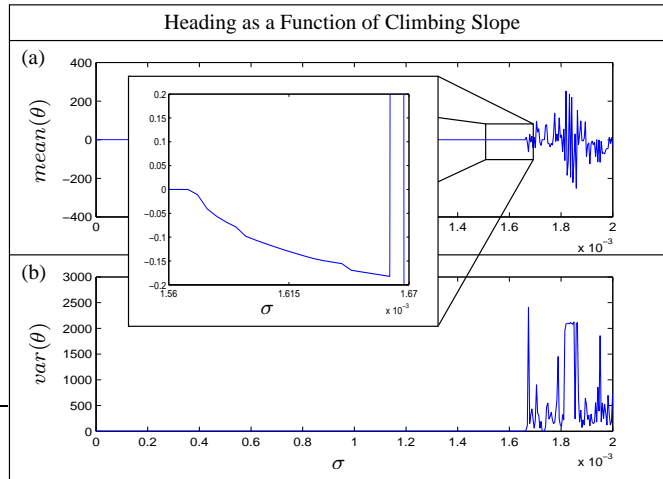
Figure 11: Mean and variance of heading as a function of climbing slope for the RiSE Configuration climber, $k = 1$, $g = 9.8$. (a) Note that the mean heading remains zero except for a small decrease in $mean(\theta)$ just before the climber falls into chaotic instability. (b) The approximate limit of stable climbing slopes is clearly illustrated with the spike in $var(\theta)$ near $\sigma = 1.56 \cdot 10^{-3}$.

gravity on a legged climber. For now, following the Raibert assumption of decoupled transverse and sagittal plane dynamics [1] we assume a stable heading and propose a model of the sagittal plane dynamics of a legged climber based on the successful SLIP template [2].

The standard flat-ground SLIP template is a pogo stick. A point-mass is mounted to the top of a massless spring leg, and control is exerted by choosing the angle of the leg relative to the level ground at touchdown. The leg angle can only be controlled during flight, when the pogo stick is airborne and ballistic, and no control is exerted during stance. The SLIP template has been used to model biological [6, 7] and robotic [13, 18, 16] systems on level ground, and has been shown in this setting to exhibit stability properties enabling the decoupled control of hopping height and forward velocity through leg touch-down angle [1, 12, 2, 4, 15, 19, 3].

In order to extend the existing SLIP model to vertical and sloped domains, we model the addition or removal of energy through a "thrust" phase during stance.

4.1 Dynamics

The body geometry and coordinate system of the 2-DOF climber is shown in Fig. 12, while the complete dynamical mode, with five phases of operation, is show in Fig. 13. The climber is assumed have a rigid body of mass m. The body acts as a point-mass mounted directly on top of the leg, eliminating pitching during stance. The leg is a massless spring of length ρ with resting length ρ_{rl}. Leg angle relative to gravity is denoted ϕ, and the leg angle at touchdown is ϕ_{TD}. The distance from the climbing slope to center of mass of the climber along world frame axis W_z is denoted z. The position of the climber center of mass in the world frame along the W_y axis is denoted y. The climber operates in a gravity field of magnitude g and climbs a surface with constant slope σ relative to gravity. We assume no energy loss in spring compression or decompression, and no friction due to drag in stance or flight. In stance we assume perfect ground attachment, meaning that the foot-ground contact is modeled as a frictionless revolute joint. Climber configuration is specified as the tuple (y, z, ϕ). No control is exerted during stance, and the only control consists of selecting ϕ_{TD}.

For our extended SLIP models we consider linear springs under finite and instantaneous thrust duration as well as two models of an "air" spring under instantaneous thrust duration. For linear springs, spring force is governed by $F = -k_i \rho$, where k_i is the spring constant. Instantaneous thrust is exerted by a discrete change in spring constant from k_1 to k_2. Finite duration thrust is exerted by stretching or compressing the spring at a constant rate r for a time δ_t. For the two models of "air" springs, spring force is governed by $F = \frac{-k_i}{\rho}$ [4] and $F = \frac{-k_i}{\rho^3}$ [15, 16]. Instantaneous thrust is again exerted by a discrete change in spring constant from k_1 to k_2. For ease of notation, we will denote the spring potential generated with spring constant k, leg length ρ, and resting leg length ρ_{rl} by $V(k, \rho, \rho_{rl})$.

In the following, we formulate the equations of motion and the switching surfaces for the extended SLIP model corresponding to each of the four spring cases: Flight, Compression, Thrust, and Decompression.
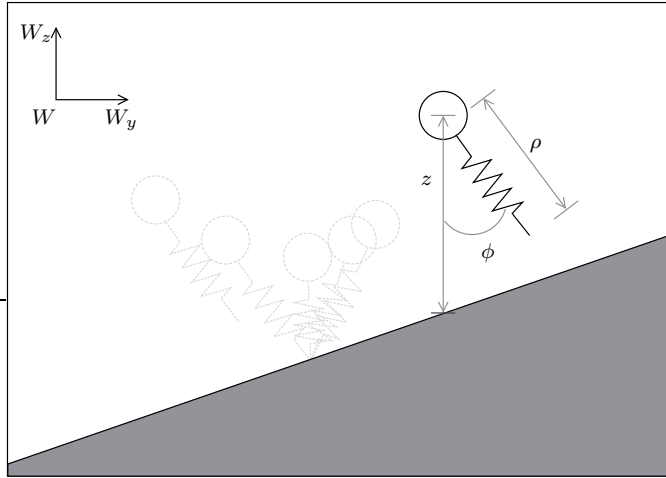
Figure 12: 2-DOF hopping climber body geometry. Position in the world frame is given in Cartesian coordinates (W_y, W_z). The gravity vector points in the $-W_z$ direction. The scalar z measures the height of the center of mass above the ground along the W_x axis. ρ measures the length of the spring-leg. The angle between the spring-leg and W_x is mesaured by ϕ.
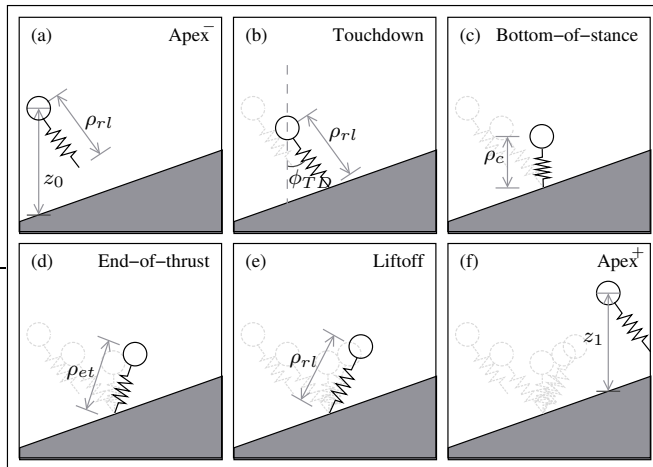
Figure 13: 2-DOF hopping climber model executing a single stride. (a) At apex in flight. (b) Touchdown. The angle of the leg relative to gravity is ϕ_{TD}. (c) The rate of leg compression has gone to zero. At this moment the climber begins exerting a thrust force. (d) After a specified thrust duration the leg behaves again like a simple unactuated spring. (e) The leg has extended to its original rest length. At this point the hopper loses contact with the ground. (f) Apex of flight.

4.1.1 Flight

During flight the hopping climber is not in contact with the ground and the leg is at its rest length. Because of our simplifying assumptions, in flight the climber behaves as a ballistic point mass in a gravity field without drag. Flight begins at liftoff, when the hopper loses contact with the ground, and ends at touchdown, when the hopper contacts the ground with downward velocity and leg at angle ϕ_{TD}.

$$\begin{bmatrix} \ddot{y} \\ \ddot{z} \end{bmatrix} = \begin{bmatrix} 0 \\ -g \end{bmatrix} \tag{16}$$

$$h_{\mathbf{f}}^{\mathbf{c}}(\mathbf{x}, t) = z - \rho_{rl}\cos(\phi_{TD}) - (y + \rho_{rl}\sin(\phi_{TD}))\sigma \tag{17}$$

4.1.2 Compression

During compression the hopper is in contact with the ground and the leg length is decreasing. Compression begins with touchdown and ends with bottom-of-stance, when the rate of leg compression goes to zero. It should be noted that the equations of motion are different for each type of spring.

$$\begin{bmatrix} \ddot{y} \\ \ddot{z} \end{bmatrix} = \frac{\partial V(k_1, \rho, \rho_{rl})}{\partial \rho} \frac{1}{m} \begin{bmatrix} -\sin(\phi_{TD}) \\ \cos(\phi_{TD}) \end{bmatrix} - \begin{bmatrix} 0 \\ g \end{bmatrix} \tag{18}$$

$$h_{\mathbf{c}}^{\mathbf{t}}(\mathbf{x}, t) = \dot{\rho} \tag{19}$$

4.1.3 Thrust

In the instantaneous thrust cases, this phase has duration 0, and we move directly to the decompression phase. In the finite thrust duration linear spring case, we imagine the leg spring being stretched or compressed independent of the actual leg length and "resting" leg length, at a rate r for a time δ_t. We denote the elapsed time since the beginning of thrust s_t.

$$\begin{bmatrix} \ddot{y} \\ \ddot{z} \end{bmatrix} = \frac{\partial V(k_1, \rho, \rho_{rl} + rs_t)}{\partial \rho} \frac{1}{m} \begin{bmatrix} -\sin(\phi_{TD}) \\ \cos(\phi_{TD}) \end{bmatrix} - \begin{bmatrix} 0 \\ g \end{bmatrix} \tag{20}$$

$$h_{\mathbf{t}}^{\mathbf{d}}(\mathbf{x}, t) = \delta_t - s_t \tag{21}$$

4.1.4 Decompression

Decompression is very similar to compression. Decompression begins at end-of-thrust and ends at liftoff, when the leg has extended to its original resting length ρ_{rl}. The equations of motion are different for each type of spring and thrust model. For the linear spring finite duration thrust model,

$$\begin{bmatrix} \ddot{y} \\ \ddot{z} \end{bmatrix} = \frac{\partial V(k_1, \rho, \rho_{rl} + r\delta_t)}{\partial \rho} \frac{1}{m} \begin{bmatrix} -\sin(\phi_{TD}) \\ \cos(\phi_{TD}) \end{bmatrix} - \begin{bmatrix} 0 \\ g \end{bmatrix} \tag{22}$$

For instantaneous thrust models,

$$\left[\begin{array}{c} \ddot{y} \\ \ddot{z} \end{array} \right] = \frac{\partial V(k_2, \rho, \rho_{rl})}{\partial \rho} \frac{1}{m} \left[\begin{array}{c} -\sin(\phi_{TD}) \\ \cos(\phi_{TD}) \end{array} \right] - \left[\begin{array}{c} 0 \\ g \end{array} \right] \tag{23}$$

$$h_{\mathbf{d}}^{\mathbf{f}}(\mathbf{x}, t) = \rho_{rl} - \rho \tag{24}$$

4.2 Intractability of the 2-DOF Hopping Climber

Attempts to analytically solve for stability conditions of this model quickly reveal the intractability of the climbing SLIP model. Unfortunately, as with flat-ground 2-DOF SLIP models, we are unable to integrate exact stance dynamics without elliptic integrals [15].

Previous efforts to circumvent the elliptic integrals in level-ground SLIP models were based on nonlinear stance approximations [15, 16], as well as exploited symmetries to asses stability of periodic orbits through return maps [12].

While in level-ground models, researchers have neglected gravity during the stance phase to aid in these approximations, we believe the gravity field must be incorporated during all phases for the extended SLIP model to accurately reflect actual physical phenomena. Further difficulties arise in our analysis because with gravity, the periodic orbits are now asymmetric – this is due simply to the fact that the robot climbs with each period. Some sort of approximation is inevitable, as we have demonstrated here that the 2-DOF model is intractable. However, we insist on an approximation which does not neglect gravity and which can accommodate the inherent asymmetry in climbing. In the next section, we propose a 1-DOF model for which tractable analysis is still possible – this model provides a novel simplification of the 2-DOF extended SLIP climber yet allows tractable analysis and provides insight into the original 2-DOF model.

5 Inclined-SLIP: 1-DOF Approximation to the 2-DOF Hopping Climber

We desire an approximation to the nonlinear 2-DOF hopping climber that allows a closed-form return map without analytically opaque elliptic integrals. Our explicit consideration of a gravity field prevents us from using level-ground approximation techniques which assume zero-gravity during stance [15, 16], or require a time reversal symmetry [12]. Surprisingly, when the climbing slope of the 2-DOF hopping climber becomes vertical, the resulting return map is closed-form and has a tractable integral. In this section we introduce this model as a 1-DOF hopping climber. We define a Poincaré section for hopping climbers, derive the 1-DOF hopping climber return map for our spring and thrust models, and explore significant stability features. Finally we present experimental evidence suggesting our analysis of the 1-DOF model is indicative of the more general 2-DOF model.
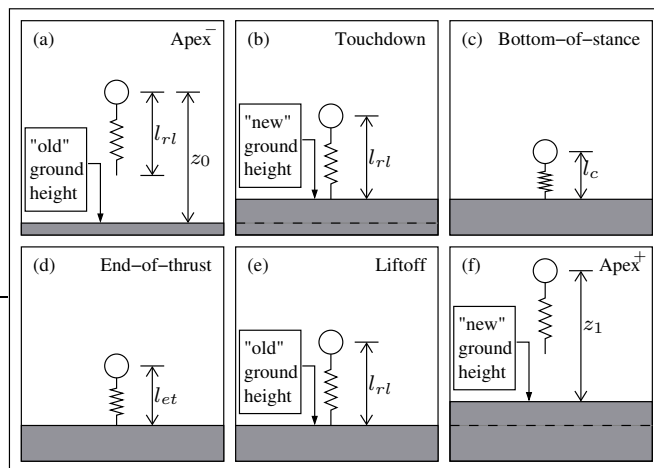
Figure 14: 1-DOF hopping climber model executing a single stride. All events are analogous to events in the 2-DOF hopping climber model. (a) Apex of flight. The ground is rising at the rate v. (b) The hopper contacts the ground. At this moment the ground instantaneously stops rising. (c) Beginning of thrust phase. (d) End of thrust phase. (e) Beginning of flight phase. At this moment the ground instantaneously resumes rising at velocity v. (f) Apex of flight.

5.1 Dynamics

The 1-DOF sagittal plane hopping climber is shown in Fig. 14, and should appear very similar to the 2-DOF hopping climber, since it is essentially the 2-DOF climber on a vertical climbing surface. Many of the assumptions about the 2-DOF hopping climber hold for the 1-DOF hopping climber. The rigid body acts like a point mass of mass m. The leg is a massless spring of length l and resting length l_{rl}. The climber operates in a gravity field of magnitude g. To approximate the coupling between horizontal and vertical progress we change the ground height n during flight by moving the ground relative to the world frame at constant velocity v. At the moment stance begins the ground instantaneously achieves zero velocity relative to the world frame. The configuration space becomes (z, n). Again, we assume no friction, no drag, and no energy loss in compression or decompression. The climber runs open-loop, and other than choosing an initial "dropping height" z_0, there is no control in flight or stance. We consider the same spring and thrust models proposed for the 2-DOF climber model. Phases and events in the 1-DOF model are analogous to those in the 2-DOF model, and purposefully named to reflect their similarity.

5.1.1 Flight

The 1-DOF flight phase differs from the 2-DOF flight phase only in that the the ground moves relative to the world frame with velocity v. Since the ground stops instantaneously on touchdown, the discrete transformation between flight and compression

22

charts is no longer the identity.

$$\dot{n} = v \tag{25}$$

$$\begin{bmatrix} \ddot{z} \\ \ddot{n} \end{bmatrix} = \begin{bmatrix} -g \\ 0 \end{bmatrix} \tag{26}$$

$$h_{\mathbf{f}}^{\mathbf{c}}(\mathbf{x}, t) = z - l_{rl} - n \tag{27}$$

$$T_{\mathbf{f}}^{\mathbf{c}} = diag(1, 1, 1, 0) \tag{28}$$

5.1.2   Compression

Compression again begins with touchdown and ends with bottom-of-stance. The ground velocity is zero, and the phase transition transformation is the identity.

$$\begin{bmatrix} \ddot{z} \\ \ddot{n} \end{bmatrix} = \begin{bmatrix} \frac{\partial V(k_1, l, l_{rl})}{\partial l} \frac{1}{m} - g \\ 0 \end{bmatrix} \tag{29}$$

$$h_{\mathbf{c}}^{\mathbf{t}}(\mathbf{x}, t) = \dot{z} \tag{30}$$

5.1.3   Thrust

Just as in the 2-DOF climber model, in the instantaneous thrust cases we skip directly to decompression. Finite thrust duration for the linear spring works just as it did in the 2-DOF model.

$$\begin{bmatrix} \ddot{z} \\ \ddot{n} \end{bmatrix} = \begin{bmatrix} \frac{\partial V(k_1, l, l_{rl} + rs_t)}{\partial l} \frac{1}{m} - g \\ 0 \end{bmatrix} \tag{31}$$

$$h_{\mathbf{t}}^{\mathbf{d}}(\mathbf{x}, t) = \delta_t - s_t \tag{32}$$

5.1.4   Decompression

Since the ground instantaneously starts moving with velocity v on liftoff, the discrete phase transition transformation is no longer the identity. For the linear spring finite thrust model,

$$\begin{bmatrix} \ddot{z} \\ \ddot{n} \end{bmatrix} = \begin{bmatrix} \frac{\partial V(k_1, l, l_{rl} + r\delta_t)}{\partial l} \frac{1}{m} - g \\ 0 \end{bmatrix} \tag{33}$$

For the instantaneous thrust models,

$$\begin{bmatrix} \ddot{z} \\ \ddot{n} \end{bmatrix} = \begin{bmatrix} \frac{\partial V(k_2, l, l_{rl})}{\partial l} \frac{1}{m} - g \\ 0 \end{bmatrix} \tag{34}$$

The threshold function and chart transformation is the same in both cases.

$$h_{\mathbf{d}}^{\mathbf{f}}(\mathbf{x}, t) = l_{rl} - (z - n) \tag{35}$$

$$T_{\mathbf{d}}^{\mathbf{f}} = diag(1, 1, 1, v) \tag{36}$$

23

5.2 Poincaré Section for the 1-DOF and 2-DOF Hopping Climbers

The Poincaré section is a surface in the phase space of a periodic system that (within certain bounds) is crossed only once per period. The relationship between the point that a trajectory leaves the Poincaré section and the point that trajectory intercepts the Poincaré section at the end of the period is referred to as a return map. Solutions to the return map of the form $\mathbf{x} = f(\mathbf{x})$ represent "fixed" points of periodic orbits.

We define the Poincaré section of our hopping climbers as lying on the hyperplane $\dot{z} = 0$. To guarantee the Poincaré section is crossed only once per stride, we restrict the surface to $z \geq n + l_{rl}$ in the 1-DOF model, and $z > (y + \rho_{rl}\sin(\phi_{TD}))\sigma + \rho_{rl}\cos(\phi_{TD})$ in the 2-DOF model. The section covers points where the hopper is at apex of flight and excludes points where the hopper is at bottom-of-stance.

Using apex of flight as our Poincaré section, a natural minimal periodic representation of our phase space is the space of height of the center of mass of the hopper above the ground and velocity of the center of mass in the world frame. Let the phase space of our 1-DOF hopper be $(z, n, \dot{z}, \dot{n})^T$ and the phase space of our 2-DOF hopper be $(y, z, \dot{y}, \dot{z})^T$. Then projections into reduced periodic space are expressed as linear transformations,

$$T_{1DOF} = \begin{bmatrix} 1 & -1 & 0 & 0 \\ 0 & 0 & 1 & 0 \\ 0 & 0 & 0 & 0 \\ 0 & 0 & 0 & 0 \end{bmatrix} \tag{37}$$

$$T_{2DOF} = \begin{bmatrix} -\sigma & 1 & 0 & 0 \\ 0 & 0 & 1 & 0 \\ 0 & 0 & 0 & 1 \\ 0 & 0 & 0 & 0 \end{bmatrix} \tag{38}$$

This Poincaré section allows us to study the stability of period-1 strides. In other words, it enables us to quantify the tendency of the climber to converge to or diverge from some configuration at apex. For the 1-DOF hopping climber we are interested in strides where the height of the climber above the ground at the end of stride is equal to the dropping height at the beginning of stride. For the 2-DOF hopping climber we are interested in strides where the height above the ground as well as the forward velocity of the climber at apex is equal to the height above the ground and forward velocity at the beginning of the stride.

5.3 1-DOF Hopping Climber Return Map

We found that for all spring and thrust models we investigated the 1-DOF hopping climber admitted a closed-form return map. This means that the dynamics of the periodic orbit can be reduced from piecewise integration over a collection of differential equations to a single difference equation.

Let z_0 be the initial height above ground at apex with t_c the time from apex to touchdown.

$$\tfrac{1}{2}gt_c^2 = z_0 - l - vt_c \quad , \quad t_c > 0 \tag{39}$$

Using the spring potential function V, height of the hopper above ground at bottom of stance can be computed from t_c.

$$\tfrac{1}{2}m(gt_c)^2 + mg(l - z_c) = V(k_1, z_c, l_{rl}) \quad , \quad z_c < l_{rl} \tag{40}$$

For the linear hopper with finite thrust, the height z_t of the hopper above ground during thrust, has a closed-from solution as a function of time.

$$\begin{aligned}
\ddot{z}_t(t) &= \frac{k_1(l_{rl} + rt - z)}{m} - g \\
\dot{z}_t(0) &= 0 \\
z_t(0) &= z_c
\end{aligned} \tag{41}$$

$$\begin{aligned}
z_t(t) = \frac{1}{k_1} \bigg(&k_1 l_{rl} - gm + k_1 rt \\
&+ (gm + k_1(z_c - l_{rl})) \cos\left(t\sqrt{\frac{k_1}{m}}\right) \\
&- r\sqrt{k_1 m} \sin\left(t\sqrt{\frac{k_1}{m}}\right) \bigg)
\end{aligned} \tag{42}$$

Knowing the position and velocity of the climber at end-of-thrust, we can compute z_a, the apex height relative to the ground height at liftoff.

$$mg(z_a - z_t) = \frac{1}{2}m\dot{z}_t^2 + V(k_1, z_t, l_{rl} + r\delta_t) - V(k_1, l_{rl}, l_{rl} + r\delta_t) \tag{43}$$

For instantaneous thrust models, z_a can be computed directly from z_c.

$$mg(z_a - z_c) = V(k_2, z_c, l_{rl}) \tag{44}$$

Now that we know the apex height, finding the time from liftoff to apex, t_a, is similar to finding the time to touchdown.

$$t_a = \frac{1}{2}gt_a^2 = z_a - l_{rl} \tag{45}$$

Finally, we can solve for the resulting hopping height, z_1, on the Poincaré section in our projected space.

$$z_1 = z_a - t_a v \tag{46}$$

Although the resulting return map is still generally difficult to analyze, numerical study shows unimodal behavior for all of our spring and thrust models. Removing gravity from our model during stance removed the unimodal behavior, resulting in entirely unstable or entirely stable fixed points for ascending and descending respectively. Contrary to studies of dynamic legged climbing in a level-ground domain, this result underscores the importance of gravity during stance in dynamic climbing. Fig. 15 illustrates return maps over a range of values for the linear spring with finite thrust duration. Note that return maps may have 0, 1, or 2 fixed points, depending on the stiffness of the linear spring. The implications for this will be discussed next.
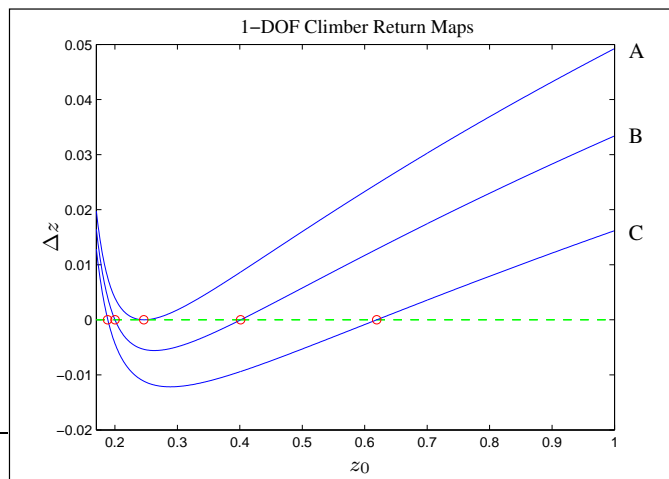
Figure 15: Return maps for a 1-DOF finite thrust linear spring climber. The climber is parameterized as $k_1 = 4500$, $r = 8$, $\delta_t = .01$, $g = 9.8$, $m = 8.5$, $l_{rl} = .1702$. The difference between hopping height and dropping height $\Delta z = z_1 - z_0$ is plotted against dropping height z_0. Solid lines are return maps. Intersections with the dashed line at $\Delta z = 0$ are fixed points. Note that two of the return maps have two fixed points, while one return map has just one fixed point. Return maps correspond to dashed lines in Fig. 16(a).

5.4 Stability of the 1-DOF Hopping Climber

In addition to finding fixed points of the return maps for our hopping climbers, we would like to know what behavior to expect if the trajectory of the hopper is perturbed from its periodic orbit. Within some neighborhood of the fixed point, a trajectory may asymptotically approach the periodic orbit, or diverge from it. One intuitive way to investigate the local stability of a fixed point is to evaluate the Jacobian of the return map at that point.

Since the return map of our vertical climber has only a single degree of freedom, the eigenvalue of the Jacobian of the return map is simply the derivative with respect to hopping height. A unimodal return map would indicate three possible configurations of fixed points for each parameterization of spring, thrust, and ground speed. Either there are two fixed points, one asymptotically stable and one unstable, one marginally stable fixed point, or no fixed points.

Fig. 16 provides a clear picture of the classification of these fixed points for an ascending climber. In the upper plot we show fixed points for a finite thrust, linear spring, climber with parameters $k_1 = 4500$, $r = 8$, $\delta_t = .01$, $g = 9.8$, $m = 8.5$, and $l_{rl} = .1702$. In the lower plot we show the eigenvalue of the Jacobian of the return map evaluated at these fixed points. We see that as the value of z_0 increases from l_{rl}, the steady-state value of v decreases quickly, then begins to increase again. Dual z_0 solutions are expected, since each cross section corresponds to a return map. It follows

26
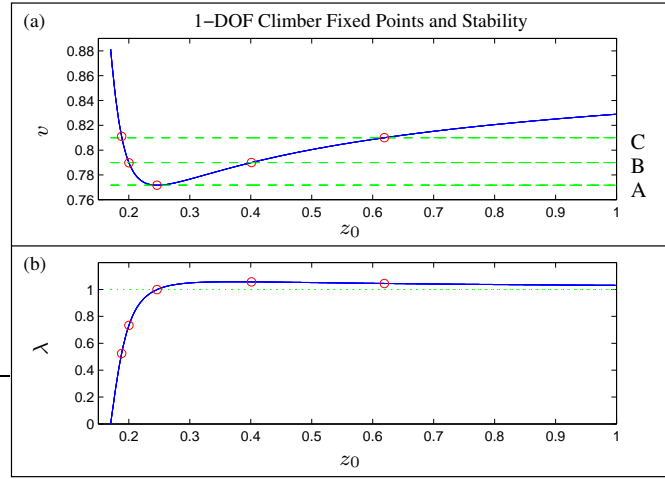
Figure 16: Fixed points and eigenvalue of the Jacobian of the return map for a finite thrust linear spring climber. $k_1 = 4500$, $r = 8$, $\delta_t = .01$, $g = 9.8$, $m = 8.5$, $l_{rl} = .1702$. (a) Rising ground rate v is plotted against dropping height z_0. The solid line represents fixed points. Horizontal slices correspond to return maps. Dashed lines represent return maps illustrated in Fig. 15. (b) Eigenvalue of the Jacobian of the return map λ is plotted against z_0.

that for each value of v that corresponds to two steady-state values of z_0, one parameterization is stable and the other is not. Indeed, looking at the plot of eigenvalues, we see that values of z_0 close to l_{rl} represent stable fixed points while larger values of z_0 represent unstable fixed points. This suggests that while ascending a slope, a climber should have an apex height close to its height at touchdown. Conversely, when descending a slope, a climber should have an apex height close to its liftoff height. Although the figure corresponds to a particular parameterization of a specific spring and thrust model, we found the features identified to be persistent over all spring and thrust models described in this paper.

5.5 Comparison of the 1-DOF Hopping Climber to the 2-DOF Hopping Climber

In this section we present empirical evidence supporting the hypothesis that the 1-DOF hopping climber captures important features of the dynamics of the 2-DOF hopping climber within some bounds.

In Fig. 17 we show a slice of the the return map of a instantaneous thrust, nonlinear $\frac{1}{\rho}$ "air" spring with $\dot{y} = .7$, $\phi_{TD} = \frac{\pi}{16}$, $k_1 = 40$, $k_2 = 50$, $\sigma = .15$, $g = 9.8$, $m = 8.5$, $\rho_{rl} = .1702$. Since the reduced dimension phase space is really three dimensional, the the return map is actually in $\mathbb{R}^4$. Because of this, the intersections shown in the return map do not represent fixed points themselves, but contours along which a fixed point might be found. The slice of the return map is acquired by projecting down to
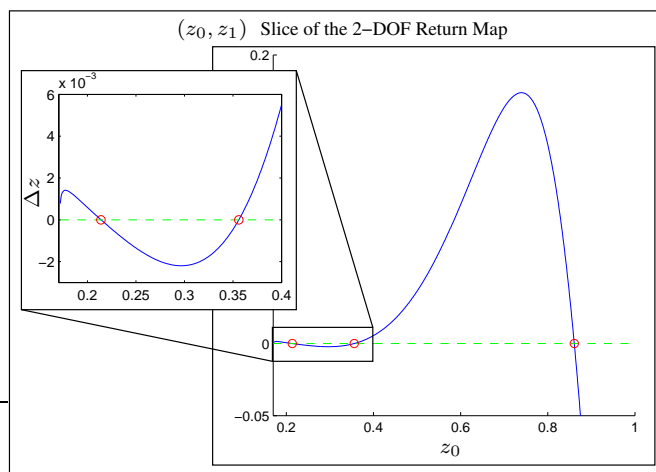
Figure 17: (z_0, z_1) slice of the 2-DOF instantaneous thrust nonlinear $\frac{1}{\rho}$ spring. The model parameters are $\dot{y} = .7$, $\phi_{TD} = \frac{\pi}{16}$, $k_1 = 40$, $k_2 = 50$, $\sigma = .15$, $g = 9.8$, $m = 8.5$, $\rho_{rl} = .1702$. $\Delta z = z_1 - z_0$. The return map actually lies in $\mathbb{R}^4$, so the dashed line represents a hyperplane of $\mathbb{R}^4$, and intersections with that dashed line correspond to contours fixed points might lie on. The section $z_0 \in [.1702, .4]$ is magnified to show similarity to the 2-DOF return map near $z_0 = \rho_{rl}$.

dimensions analogous to "dropping height" and "apex height" in the 1-DOF hopping climber. In Fig. 17 the (z_0, z_1) slice of the return map near $z_0 = \rho_{rl}$ is reminiscent of the shape of the 1-DOF return map. In other words, this figure suggests that where the dropping height is reasonably near the spring-leg rest length, the 2-DOF climber has a hopping height stability behavior similar to the 1-DOF climber.

Fig. 18 explicitly examines fixed points of the 2-DOF hopping climber. Let ξ be the height of the center of mass of the hopper directly above the ground. In Fig. 18 $\phi_{TD} = \frac{\pi}{16}$, $k_1 = 40$, $k_2 = 50$, $g = 9.8$, and $\rho_{rl} = .1702$. In the 1-DOF approximation the coupling between $\dot{y}$ and σ (forward velocity and ground slope) is modeled as the rising ground rate v. The top plot shows shows the $\dot{y}$ component of the fixed point as a function of z_0, and the middle plot shows the ground slope that corresponds to that fixed point. Although σ increases monotonically with z_0, the unimodal relationship between z_0 and $\dot{y}$ resembles the mapping between z_0 and v in the 1-DOF hopping climber shown in Fig. 16. In other words, for fixed points in the 2-DOF hopping climber, although climbing slope monotonically increases with dropping height, the coupling and between forward velocity and dropping height can be understood as similar to the coupling between rising ground velocity and dropping height for the 1-DOF hopping climber. Finally, the lower plot shows the nonzero eigenvalues of the $(\dot{y}, \xi)$ Jacobian. This plot shows greater coupling between z_0 and $\dot{y}$ for larger values z_0, which correlates with destabilizing effect of increasing z_0 in the 1-DOF model. As dropping height increases, forward velocity has a greater effect on apex height. This also suggests that for small values of z_0, *i.e.* the stable region predicted by the 1-DOF model, a simple

28
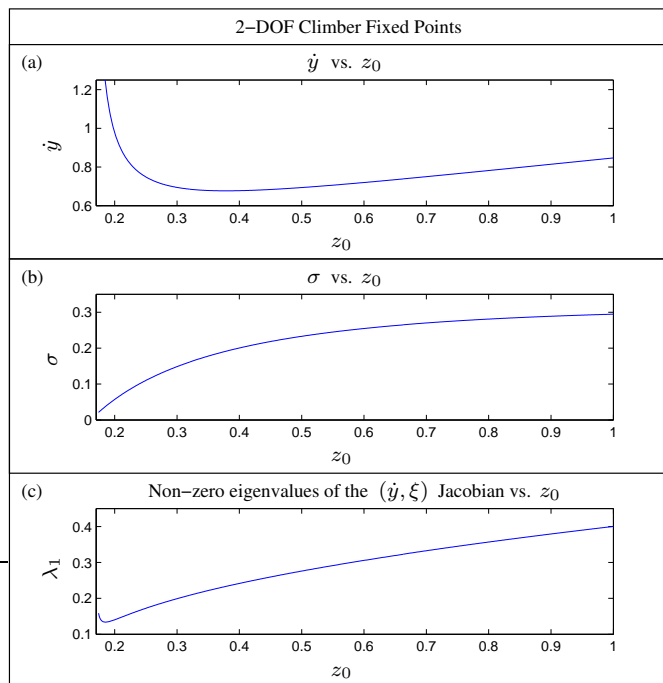
Figure 18: Fixed points of the 2-DOF instantaneous thrust nonlinear $\frac{1}{\rho}$ spring. $\phi_{TD} = \frac{\pi}{16}$, $k_1 = 40$, $k_2 = 50$, $g = 9.8$, $m = 8.5$, $\rho_{rl} = .1702$. (a) $\dot{y}$ is plotted against z_0. The coupling between $\dot{y}$ and z_0 is similar to the coupling between v and z_0 in the 1-DOF climber shown Fig. 16(a). (b) σ appears monotonic in z_0. (c) Nonzero eigenvalues of the $(\dot{y}, \xi)$ Jacobian plotted against z_0.

Raibert-like controller, which assumes forward velocity and apex height are decoupled, may be effective [19, 3, 4].

6 Conclusion and Future Work

The analytic and experimental results in Sections 3, 4, and 5 provide initial forays into the problem of legged climbing on a slope. In particular, our results indicate that it is not enough to merely apply flat-ground models to a robot on an incline – we have demonstrated that gravity must be explicitly included in the modeling for the analysis to be representative of actual physical behaviors.

The LLS and SLIP templates have been successful in modeling legged locomotion on level ground; however their naive application to a sloped domain introduces many complexities. Although the peg-leg LLS template does offer global heading stability, the asymptotically stable fixed point only allows for descending. This suggests the need for a more complex transverse plane model, and is confirmed by a brief empirical exploration of the simple planar hexapod. Approaching the dynamic legged climbing

problem from the sagittal plane, a simple modification of the SLIP template yields an intractable 2-DOF hopping climber; however constraining this model to a 1-DOF vertical climber yields an analytically tractable model with an interesting unimodal return map. Numerical study of the 2-DOF hopping climber shows stability properties similar to to those resulting from 1-DOF vertical climbing. The 1-DOF vertical climber can be used as an approximation to the 2-DOF hopping climber, indicating the usefulness of a simple Raibert controller in legged climbing

Further work may branch in a few different directions. For the inclined-LLS models, we would like to investigate the dynamics of the simple hexapod. Bifurcations with a large basin of attraction are key to the interesting dynamical behavior in the simple hexapod; however we do not have a good understanding of the underlying mechanism of these bifurcations. It would be useful to distill an even simpler model from the hexapod for both RHex and RiSE gait modifications.

For the inclined-SLIP models, the 1-DOF climbing model may be pursed both as an approximation to the 2-DOF hopping climber and as an independent model of vertical climbing. As an approximation, we would like to develop explicit bounds in the 2-DOF system where the approximation is appropriate. We assert that our analysis of the 1-DOF model suggests a Raibert controller [19, 3, 4] may be used to control a 2-DOF hopping climber. Future work might address the effect of ground slope on the size of the basin of attraction for that type of controller. Seen as a model of vertical climbing, the 1-DOF hopping climber could be the subject of future analytic study. It may be useful to further develop a precise mathematical classification of spring and thrust models that produce the stability properties outlined in this paper.

Finally, we would like to pursue the coupling between transverse and sagittal plane dynamics of full dimensional climbers as a function of gravity magnitude and climbing slope. This may be addressed through empirical study of RHex [11] and RiSE [20] using controllers developed from this paper.

7   Acknowledgements

References

[1] M. H. Raibert, *Legged Robots That Balance*. Cambridge, Massachusetts: The MIT Press, 1986.

[2] D. E. Koditschek and M. Bühler, "Analysis of a simplified hopping robot," *The International Journal of Robotics Research*, vol. 10, no. 6, pp. 587–605, 1991.

[3] A. Vakakis, J. Burdick, and T. Caughey, "An 'interesting' strange attractor in the dynamics of a hopping robot," *The International Journal of Robotics Research*, vol. 10, no. 6, pp. 606–618, 1991.

[4] R. T. M'Closkey and J. W. Burdick, "Periodic motions of a hopping robot with vertical and forward motion," *The International Journal of Robotics Research*, vol. 12, no. 3, pp. 197–218, 1993.

[5] R. M. Alexander, "Three uses for springs in legged locomotion," *The International Journal of Robotics Research*, vol. 9, no. 2, pp. 53–61, 1990.

[6] R. Blickhan and R. Full, "Similarity in multilegged locomotion: Bouncing like a monopode," *Journal of Comparative Physiology*, vol. 173, pp. 509–517, 1993.

[7] R. Full and D. Koditschek, "Templates and anchors: Neuromechanical hypotheses of legged locomotion on land," *The Journal of Experimental Biology*, vol. 202, pp. 3325–3332, 1999.

[8] R. J. Full, T. Kubow, J. Schmitt, P. Holmes, and D. Koditschek, "Quantifying dynamic stability and maneuverability in legged locomotion," *Integrative and Comparative Biology*, vol. 42, pp. 149–157, 2002.

[9] J. Schmitt and P. Holmes, "Mechanical models for insect locomotion: Dynamics and stability in the horizontal plane I. Theory," *Biological Cybernetics*, vol. 83, pp. 501–515, 2000.

[10] J. E. Seipel, P. J. Holmes, and R. J. Full, "Dynamics and stability of insect locomotion: a hexapedal model for horizontal plane motions," *Biological Cybernetics*, vol. 91, pp. 76–90, 2004.

[11] U. Saranli, M. Buehler, and D. E. Koditschek, "RHex: A simple and highly mobile hexapod robot," *The International Journal of Robotics Research*, vol. 20, no. 7, pp. 616–631, 2001.

[12] R. Altendorfer, D. E. Koditschek, and P. Holmes, "Stability analysis of legged locomotion models by symmetry-factored return maps," *The International Journal of Robotics Research*, vol. 23, no. 10-11, pp. 979–999, 2004.

[13] ——, "Stability analysis of a clock-driven rigid-body SLIP model for RHex," *The International Journal of Robotics Research*, vol. 23, no. 10-11, pp. 1001–1012, 2004.

[14] J. Schmitt and P. Holmes, "Mechanical models for insect locomotion: Dynamics and stability in the horizontal plane-II. Application," *Biological Cybernetics*, vol. 83, pp. 517–527, 2000.

[15] W. J. Schwind and D. E. Koditschek, "Characterization of monopod equilibrium gaits," in *Proceedings of the 1997 IEEE International Conference on Robotics and Automation*, 1997, pp. 1986–1992.

[16] W. Schwind and D. Koditschek, "Approximating the stance map of a 2-DOF monoped runner," *Journal of Nonlinear Science*, vol. 10, pp. 533–568, 2000.

[17] T. Kubow and R. Full, "The role of the mechanical system in control: A hypothesis of self-stabilization in hexapedal runners," *Philosophical Transactions: Biological Sciences*, vol. 354, no. 1385, pp. 849–861, May 1999.

31

[18] U. Saranli, W. J. Schwind, and D. E. Koditschek, "Toward the control of a multi-jointed, monoped runner," in *Proceedings of the 1998 IEEE International Conference on Robotics & Automation*, 1998, pp. 2676–2682.

[19] W. J. Schwind and D. E. Koditschek, "Control of forward velocity for a simplified planar hopping robot," in *IEEE International Conference on Robotics and Automation*, 1995, pp. 691–696.

[20] K. Autumn, M. Buehler, M. Cutkosky, R. Fearing, R. J. Full, D. Goldman, R. Groff, W. Provancher, A. A. Rizzi, U. Saranli, A. Saunders, and D. E. Koditschek, "Robotics in scansorial environments," G. R. Gerhart, C. M. Shoemaker, and D. W. Gage, Eds., vol. 5804, no. 1.   SPIE, 2005, pp. 291–302. [Online]. Available: http://link.aip.org/link/?PSI/5804/291/1